RSC Advances

PAPER

View Article Online
View Journal | View Issue

Cite this: *RSC Adv.*, 2023, **13**, 632

Synthesis of rGO supported Cu@FeCo catalyst and catalytic hydrolysis of ammonia borane†

Fangyuan Qiu, [acd] Xiang Hao,[a] Wanyou Huang,*[acd] Yanling Wu, [a] Ruixia Chu,[acd] Jun Yang,[acd] Wenjun Fu,[acd] Guohong Ren,[ad] Chuanyan Xu[acd] and Wujisiguleng Bao*[b]

Received 19th October 2022
Accepted 4th December 2022

DOI: 10.1039/d2ra06606h

rsc.li/rsc-advances

Highly dispersed Cu@FeCo/rGO catalysts have been prepared by two-step reduction method and used for hydrogen production from ammonia borane (NH_3BH_3, AB) hydrolysis at 298 K. The activity and reusability of synthesized composite catalyst were much more higher than Cu@FeCo for AB hydrolysis dehydrogenation at 298 K. Kinetic study manifested that AB hydrolysis dehydrogenation with Cu@FeCo/rGO catalysts was approaching to the first order at different catalyst concentrations. The hydrolysis reaction completed within four minutes, and its maximum hydrogen production rate reached to 7863.0 ml min^{-1} g^{-1} at 298 K.

1. Introduction

Hydrogen is considered as an outstanding alternative to meet the growing requirements for clean power in vehicle application.[1–4] Ammonia borane (AB) is one of the most prospective materials for hydrogen storage owning to the high hydrogen content (19.6%) and its stability in aqueous solutions.[5–7] AB hydrolysis reaction equation is expressed as below. $NH_3BH_3 + 2H_2O \rightarrow NH_4^+ + BO_2^- + 3H_2\uparrow$. Nevertheless, if there is no catalyst, hydrolysis reaction rate of AB is slow at 298 K.[8,9] Therefore, to get more hydrogen energy from the AB hydrolysis reaction, it is essential to find a suitable catalyst. So far, many catalysts have been studied to help release hydrogen from AB.[10–14] With the application of nano catalysts in AB hydrolysis, non noble metal catalysts are judged to a prospective choice as a result of their low cost, novel structure, electronic properties and magnetic properties.[15–20] Considering the influence of structure on catalytic activity, core–shell catalysts fascinate many researchers.[21–24] They present higher catalytic activity than those with no core–shell structure. This may be caused by the formation of more and more active sites of catalyst surface. However, the investigation of the core–shell catalysts shows that their catalytic properties are closely related to the dispersion of core–shell metal nanoparticles (NPs).[25–29] Therefore, the agglomeration of particles on account of their high surface energy and magnetism is the key obstacle to the evolution. Many methods have been tried to improve the accumulation of the NPs. Various carriers have been widely used to prepare well-dispersed catalysts.[6,30–34] As we all know, graphene is a special carbon material with single atom thickness with a large surface area and a high density of free electron. As a desirable carrier material, it can make metal NPs to disperse well in absence of surfactant.[35] So far, metal NPs loaded onto graphene have been primarily prepared by one-step and two-step reduction methods. In former method, there is simultaneous reduction of metal ions and graphene oxide (GO), while in latter method, GO is first reduced to produce reduced graphene (rGO), and then metal ions fixed on rGO. Yet simple one-step reduction method hasn't been universally adopted in AB hydrolysis reaction. It is difficult to separate GO and metal salt because they both consume reducing agent. It is well known that during catalytic hydrolysis of AB by one-step reduction method, the accurate value of reducing agent is very important. This can have a direct impact on activity of catalyst, for instance, hydrogen production rate and catalytic reaction time. Opposite of this, in the two-step reduction method, these problems could be successfully avoided by means of reducing metal ions and GO respectively.

In the prior study, Cu@FeCo catalyst owned good activity for hydrolysis of AB,[23] but agglomeration phenomena of the core–shell catalysts has led to a serious decline in reusability. Therefore, in this study, we used a two-step reduction method to prepare Cu@FeCo/rGO catalyst to increase its dispersion and catalytic activity for AB hydrolysis.

[a]*Departments of Energy and Power Engineering, Automotive Engineering College, Shandong Jiaotong University, Ji Nan 250357, China. E-mail: nankaiqfy@126.com*

[b]*College of Mathematics and Physics, Inner Mongolia Minzu University, Tong Liao, Inner Mongolia, 028043, China*

[c]*Intelligent Testing and High-end Equipment of Automotive Power Systems Shandong Province Engineering Research Center, Ji Nan 250357, China*

[d]*Key Laboratory of Transportation Industry for Transport Vehicle Detection, Diagnosis and Maintenance Technology, Ji Nan 250357, China*

† Electronic supplementary information (ESI) available: An online version of this article provides additional data related to this article. Correspondence and requests for the material may be sent to F.-Y. Qiu. See DOI: https://doi.org/10.1039/d2ra06606h

2. Experimental section

2.1. Preparation process of rGO

First, we employ the modified Hummers' method to prepare GO.[36] And then, it was put into a furnace in the atmosphere of 10% H_2–Ar, during which reaction temperature was slowly increased to 1073 K with a rate of 10 K min^{-1} and holded for one minute. And finally, rGO was obtained.

2.2. Preparation of Cu@FeCo/rGO and its application in hydrolysis reactions of AB

For synthesis of Cu@FeCo/rGO, deionized water (10 ml) and rGO were sonicated for ten minutes, and then a uniform solution was formed. After that, a mixture of $CuCl_2$–$2H_2O$ (Alfa Aesar, 99+%), $CoCl_2$–$6H_2O$ (Alfa Asear, 98.0–102.0%) and $FeSO_4$–$7H_2O$ (Alfa Asear, 99+%) was mixed with the above solution and then continued to sonicate for ten minutes at 298 K. The molar ratio of Cu : Fe : Co was maintained at 3 : 1 : 6. Theoretically, the content of Cu@FeCo in Cu@FeCo/rGO is 50 wt%, which remains unchanged. Then, the uniform solution was added to a double round-bottom flask, which contained 63 mg of AB (Sigma-Aldrich, 90%). It was realized by assist of a pressure equalizing funnel, which was attached to a mouth of the round bottom flask. The other mouth was closely connected with the gas burette. Hydrolysis reaction occurred accompanied by the above mixed solution put in the round bottom flask and stirred. The produced gas volume was measured by water displacement employing the gas burette until the reaction was over. The sign of the end of the reaction was that the molar ratio of hydrogen to AB was infinitely near to 3.0. In the process of product chemical cleaning, washing and filtering by deionized water and anhydrous ethanol for three times were necessary. Catalyst was dried under vacuum at 333 K continuing near to 4 h before testing. Experiments under variable catalyst concentrations were also made.

Characterization measurement methods are described in ESI.†

3. Results and discussion

3.1. Characterization of Cu@FeCo/rGO

Micromorphological inspection of the composite catalysts was comprehensively carried out by TEM observation. It can be clearly seen that the agglomeration of Cu@FeCo nanocatalysts was serious in Fig. 1a. In contrast, Fig. 1b showed that the agglomeration phenomenon was significantly improved after loading the catalyst onto graphene with a lamellar structure. These catalysts can be evenly dispersed on the rGO plate. Thus, it can be assumed that the dispersion effect of rGO on the catalyst was very great. This striking property of graphene indicated that it was an excellent carrier material for Cu@FeCo nanocatalysts. Additionally, phase structure of catalysts was characterized by X-ray diffraction (XRD) (Fig. 2). The diffraction pattern of rGO showed that its strongest diffraction peak appeared near $2\theta = 26.5°$, which was attributed to (002) reflection. However, in the Cu@FeCo/rGO composite catalyst, the intensity of this diffraction peak was significantly weakened. Combined with the TEM analyses, it can be derived that Cu@FeCo nanocatalysts were successfully loaded onto the lamellar structure of rGO.

FTIR spectra detection results were shown in Fig. 3. From GO, a broad and strong band appeared on an absorption peak of 3429.4 cm^{-1}, which was attributed to the hygroscopic nature of GO. Meanwhile, the absorption peak appearing at 1737.2 cm^{-1} was relatively weak, which was due to the C=O stretching vibration in the carbonyl or carboxyl group. The peak appearing at 1630.9 cm^{-1} was associated with vibration of absorbing water molecule and the skeletal vibration of the unoxidized graphite domains. The bands appearing at 1391.9 cm^{-1} and 1090.5 cm^{-1} were related to the O–H vibrations in the carboxylic acid and the

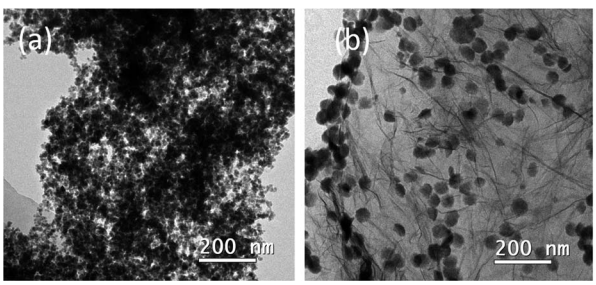

Fig. 1 TEM images for (a) Cu@FeCo and (b) Cu@FeCo/rGO.

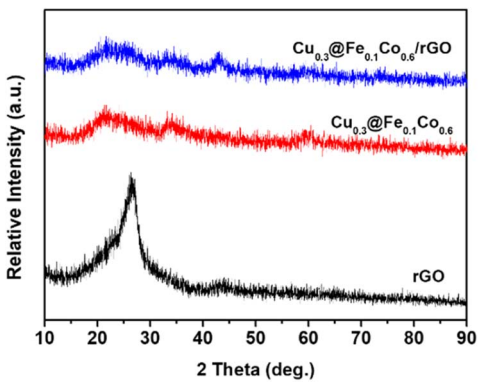

Fig. 2 XRD patterns of rGO, Cu@FeCo and Cu@FeCo/rGO.

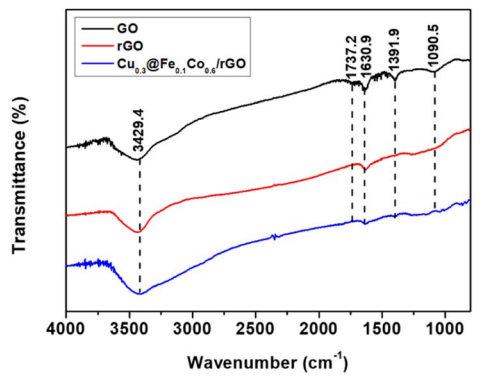

Fig. 3 FTIR spectra of GO, rGO and Cu@FeCo/rGO.

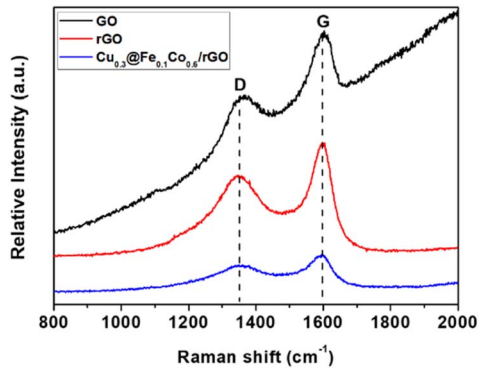

Fig. 4 Raman spectra of GO, rGO and Cu@FeCo/rGO.

distortion of the C–O bands, respectively. Compared to GO, it is noteworthy that the above absorption peaks were not significant in rGO and Cu@FeCo/rGO. It fully proved that GO was reduced.[37]

Raman spectra (Fig. 4) manifested that GO, rGO and Cu@FeCo/rGO had similar characteristic peaks, which appeared at 1351.8 cm^{-1} (D band) and 1599.6 cm^{-1} (G band). The D-band identified that the disorder originated from epoxide and hydroxyl groups on the carbon basal plane or edge, while the G-band was attributed to the stretching vibration of graphitic C(sp^2)–C(sp^2) bond.[38] Yet difference of the intensity ratio (I_D/I_G) between the D and G bands among them also existed. It represented the defect density and the degree of graphitization of the carbonaceous material.[39] It's obvious that the I_D/I_G of rGO was high in comparision with GO, which confirmed that GO was reduced. For comparison, the increase in I_D/I_G of Cu@FeCo/rGO indicated that reducing agent (AB) and Cu@FeCo both promoted reduction of GO.

3.2. Catalytic activities of Cu@FeCo/rGO for the hydrolysis of AB

To determine the activity of Cu@FeCo/rGO in hydrogen production from hydrolysis of AB, hydrogen production rate was determined in a typical calibrated buret system filled with water at 298 K (Fig. 5). It was obvious that precipitation of hydrogen was fast and linear when the catalytic reaction started.

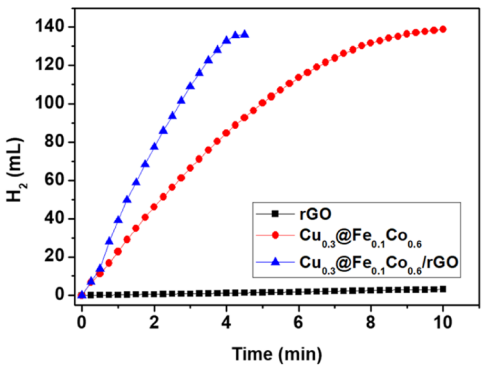

Fig. 5 rGO, Cu@FeCo and Cu@FeCo/rGO catalytic hydrogen production from AB hydrolysis.

The maximum hydrogen production rate of AB hydrolysis under the catalysis of the above catalysts was displayed in Table 1 (at 298 K). Obviously, compared with $Cu_{0.3}@Fe_{0.1}Co_{0.6}$ and rGO, $Cu_{0.3}@Fe_{0.1}Co_{0.6}$/rGO catalysts owned better catalytic activity. The maximum rate of hydrogen production was 7863.0 ml min^{-1} g^{-1} at 298 K, which was much higher than $Cu_{0.3}@Fe_{0.1}Co_{0.6}$ (6674.2 ml min^{-1} g^{-1}).[23] The catalytic hydrolysis reaction ended within four minutes. Notably, the catalytic activity of rGO for AB hydrolysis was poor, with hydrogen production rate of only 27.6 ml min^{-1} g^{-1} at 298 K (Table 1). And just 4.6 ml H_2 released during fifteen minutes. Thus, the improved catalytic activity of Cu@FeCo/rGO for AB hydrolysis was mainly attributed to Cu@FeCo dispersing on graphene lamellar structure, which also increased catalytic activity by exposing more active sites of the catalyst.

Further experiments were conducted to investigate the kinetic performance of Cu@FeCo/rGO catalyst in AB hydrolysis reaction. Fig. 6 showed the variation curve of the volume of hydrogen

Table 1 The maximum hydrogen production rate of AB hydrolysis with the catalysis of rGO, Cu@FeCo and Cu@FeCo/rGO at 298 K

Catalyst	Maximum hydrogen production rate (ml min^{-1} g^{-1})
rGO	27.6
$Cu_{0.3}@Fe_{0.1}Co_{0.6}$	6674.2
$Cu_{0.3}@Fe_{0.1}Co_{0.6}$/rGO	7863.0

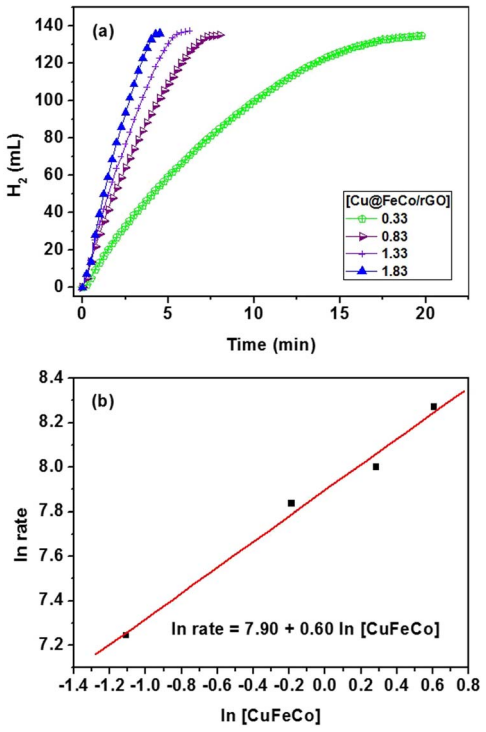

Fig. 6 (a) Relationship between time and hydrogen volume generated by hydrolysis of AB catalyzed by Cu@FeCo/rGO with variable catalyst concentrations [AB] [200 mM], T (298 K), (b) log scale diagram of hydrogen production rate and catalyst concentration.

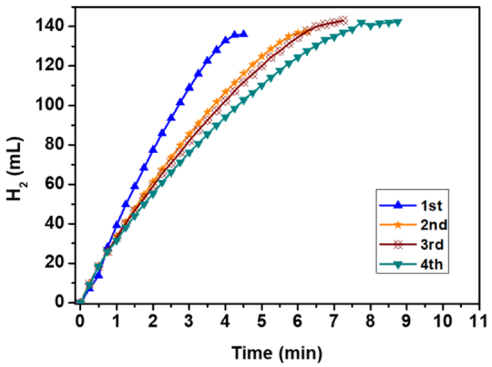

Fig. 7 Hydrogen generated from the hydrolysis reaction of AB catalyzed by Cu@FeCo/rGO for reusability test at 298 K.

produced with the reaction time during hydrogen liberation from AB hydrolysis under the catalytic effect of Cu@FeCo/rGO with variable catalyst concentrations ([AB] = 200 mM). In the curve of Fig. 6a, it can be seen that the hydrogen was produced rapidly and linearly. The slope of the curve between hydrogen production rate and catalyst concentration (Fig. 6b) was about 0.60. It showed that the hydrolysis reaction of AB was close to the first order related to Cu@FeCo/rGO catalyst concentration.

The cycle stability test experiment of Cu@FeCo/rGO in the hydrolysis of AB was conducted at 298 K. Compared with Cu@FeCo catalyst,[23] it was worth noting that the catalyst still had good cycle stability after four cycles (Fig. 7).

4. Conclusions

To sum up, we have successfully synthesized well dispersed Cu@FeCo/rGO adopting two-step reduction method. Cu@FeCo/rGO catalyst has satisfactory activity in catalytic hydrolysis of AB and the advantages of magnetic reuse. Hydrolysis reaction can be completed quickly within four minutes at 298 K, and the maximum hydrogen production rate was 7863.0 ml min^{-1} g^{-1}. The enhancement of activity shows that rGO is a prospective carrier of metal catalysts used in AB hydrolysis.

Author contributions

Writing—original draft and writing, F. -y. Q.; investigation, X. H.; data curation, R. -x. C.; review & editing, W. -y. H.; data processing, J. Y.; supervision, W. -j. F.; funding acquisition, G. -h. R.; resources, Y. -l. W.; management & funding, C. -y. X.; financial support, W. B. All authors have read and agreed to the published version of the manuscript.

Conflicts of interest

There are no conflicts to declare.

Acknowledgements

This work was financially supported by the Doctoral Scientific Research Foundation of Shandong Jiaotong University (BS201902005, BS2020001), the Natural Science Foundation of Shandong Province (ZR2022ME096, ZR2021QB181, ZR2020ME126), the Transportation Department Foundation of Shandong Province (2020B94), Undergraduate Teaching Reform Research Project of Shandong Jiaotong University (2022YB05) and Inner Mongolia Minzu University doctoral research startup fund (No. BS484). The authors would like to thank MJEditor (http://www.mjeditor.com) for its linguistic assistance during the preparation of this manuscript.

References

1 Y. N. Wu, F. T. Liu, J. M. He, M. Wu and Y. M. Ke, Obstacle identification, analysis and solutions of hydrogen fuel cell vehicles for application in China under the carbon neutrality target, *Energy Policy*, 2021, **159**, 112643.
2 C. Z. Zhang, X. J. Cao, P. Bujlo, B. Chen, X. Zhang, X. F. Sheng and C. Liang, Review on the safety analysis and protection strategies of fast filling hydrogen storage system for fuel cell vehicle application, *J Energy Storage*, 2022, **45**, 103451.
3 J. Mei, X. T. Wang and J. L. Kirtley, Optimal scheduling of real multi-carrier energy storage system with hydrogen-based vehicle applications, *IET Renew. Power Gener.*, 2019, **14**, 381–388.
4 M. J. Hülsey, V. Fung, X. D. Hou, J. S. Wu and N. Yan, Hydrogen spillover and its relation to hydrogenation: observations on structurally defined single-atom sites, *Angew. Chem., Int. Ed.*, 2022, **61**, e202208237.
5 Q. Wang, F. Y. Fu, A. Escobar, S. Moya, J. Ruiz and D. Astruc, Click dendrimer-stabilized nanocatalysts for efficient hydrogen release upon ammonia-borane hydrolysis, *ChemCatChem*, 2018, **10**(12), 2673–2680.
6 L. M. Luo, M. Yang and G. W. Chen, Continuous synthesis of TiO_2-supported noble metal nanoparticles and their application in ammonia borane hydrolysis, *Chem. Eng. Sci.*, 2022, **251**, 117479.
7 J. J. Chen, H. S. Cai and T. X. Zhao, Solid-state mechanochemical synthesis of Rh/Al_2O_3 catalysts for effective hydrolysis of ammonia borane, *Mol. Catal.*, 2022, **528**, 112518.
8 M. P. Ye, J. Wu and G. Y. Fan, Hierarchical porous cobalt/carbon hybrid anchored Ru-catalyzed ammonia-borane hydrolysis for efficient H_2 release, *Fuel*, 2022, **321**, 123982.
9 J. S. Wang, Y. Y. Yu, W. K. Xu, H. Yu, W. W. Zhang, H. L. Huang, G. R. Zhang and D. H. Mei, Covalent triazine framework encapsulated Pd nanoclusters for efficient hydrogen production *via* ammonia borane hydrolysis, *J. Catal.*, 2022, **411**, 72–83.
10 Y. T. Li, J. Y. Meng, Y. Zhu, Y. P. Yang and X. L. Zhang, Ultrafine Ru nanoparticles confined in graphene-doped porous g-C_3N_4 for effectively boosting ammonia borane hydrolysis, *Colloids Surf., A*, 2022, **649**, 129513.
11 J. X. Liu, M. Yang, R. F. Jiang, X. C. Zheng and P. Liu, Hexagonal boron nitride supported ruthenium nanoparticles as highly active catalysts for ammonia borane hydrolysis, *Int. J. Hydrogen Energy*, 2021, **46**, 17708–17719.

12 J. P. Zhang, J. Li, L. J. Yang, R. Li, F. M. Zhang and H. Dong, Efficient hydrogen production from ammonia borane hydrolysis catalyzed by TiO_2-supported RuCo catalysts, *J. Hydrogen Energy*, 2021, **46**, 3964–3973.

13 H. Wu, Y. J. Cheng, Y. P. Fan, X. M. Lu, L. X. Li, B. Z. Liu, B. J. Li and S. Y. Lu, Metal-catalyzed hydrolysis of ammonia borane: Mechanism, catalysts, and challenges, *J. Hydrogen Energy*, 2020, **45**, 30325–30340.

14 M. Aksoy, S. E. Korkut and Ö. Metin, The rational design of gCN/a-WOx/Pt heterostructured nanophotocatalysts for boosting the hydrogen generation from the hydrolysis of ammonia borane under visible light, *J. Hydrogen Energy*, 2022, DOI: **10.1016/j.ijhydene.2022.06.186**.

15 J. L. Zhou, X. J. Feng, Y. F. Zhao, R. Q. Cui, D. Wang and B. Zhang, Noble-metal-free CuNi/Co_3O_4 hybrid nanosheets as efficient and magnetically recyclable catalysts for hydrolysis of ammonia borane, *J. Alloys Compd.*, 2022, **923**, 166345.

16 F. M. Zhang, R. Li, J. P. Zhang and H. Dong, KCC-1 supported CuCo bimetal catalysts for promoting hydrogen production from ammonia borane hydrolysis, *Catal. Lett.*, 2022, **152**, 2832–2839.

17 S. Özkar, Magnetically separable transition metal nanoparticles as catalysts in hydrogen generation from the hydrolysis of ammonia borane, *J. Hydrogen Energy*, 2021, **46**, 21383–21400.

18 M. Asim, S. G. Zhang, Y. T. Wang, B. Maryam, M. Sajid, C. X. Shi, L. Pan, X. W. Zhang and J. J. Zou, Self-supporting NiCoP for hydrogen generation *via* hydrolysis of ammonia borane, *Fuel*, 2022, **318**, 123544.

19 Y. F. Feng, J. Y. Liao, X. D. Chen, H. Z. Wang, B. S. Guo, H. Li, L. Zhou, J. Huang and H. Li, Synthesis of rattle-structured $CuCo_2O_4$ nanospheres with tunable sizes based on heterogeneous contraction and their ultrahigh performance toward ammonia borane hydrolysis, *J. Alloys Compd.*, 2021, **863**, 158089.

20 J. Chen, B. Long, H. B. Hu, Z. Q. Zhong, I. Lawa, F. Zhang, L. W. Wang and Z. H. Yuan, Synthesis of a novel Co–B/CuNWs/CTAB catalyst *via* chemical reaction at room temperature for hydrolysis of ammonia-borane, *J. Hydrogen Energy*, 2022, **47**, 2976–2991.

21 C. Wang, H. L. Wang, Z. L. Wang, X. J. Li, Y. Chi, M. G. Wang, D. W. Gao and Z. K. Zhao, Mo remarkably enhances catalytic activity of Cu@MoCo core-shell nanoparticles for hydrolytic dehydrogenation of ammonia borane, *J. Hydrogen Energy*, 2018, **43**, 7347–7355.

22 C. Wang, Z. L. Wang, H. L. Wang, Y. Chi, M. G. Wang, D. W. Cheng, J. J. Zhang, C. Wu and Z. K. Zhao, Noble-metal-free Co@Co_2P/N-doped carbon nanotube polyhedron as an efficient catalyst for hydrogen generation from ammonia borane, *J. Hydrogen Energy*, 2021, **46**, 9030–9039.

23 F. Y. Qiu, Y. L. Dai, L. Li, C. C. Xu, Y. N. Huang, C. C. Chen, Y. J. Wang, L. F. Jiao and H. T. Yuan, Synthesis of Cu@FeCo core-shell nanoparticles for the catalytic hydrolysis of ammonia borane, *J. Hydrogen Energy*, 2014, **39**, 436–441.

24 J. R. Huo, L. Fu, C. X. Zhao and C. Z. He, Hydrogen generation of ammonia borane hydrolysis catalyzed by Fe22@Co58 core-shell structure, *Chin. Chem. Lett.*, 2021, **32**, 2269–2273.

25 Q. H. Nguyen, K. Im and J. Kim, Synthesis of hollow Fe, Co, and N-doped carbon catalysts from conducting polymer-metal-organicframeworks core-shell particles for their application in an oxygen reduction reaction, *J. Hydrogen Energy*, 2022, **47**, 24169–24178.

26 X. Cai, R. Lin, X. Liu and Y. C. Zhao, Effect of heat treatment on the surface structure of Pd@Pt–Ni core-shell catalysts for the oxygen reduction reaction, *J. Alloys Compd.*, 2021, **884**, 161059.

27 J. Kong, Y. H. Qin, T. L. Wang and C. W. Wang, Pd_9Au_1@Pt/C core-shell catalyst prepared *via* Pd_9Au_1-catalyzed coating for enhanced oxygen reduction, *J. Hydrogen Energy*, 2020, **45**, 27254–27262.

28 Y. Sohn, N. Jung, M. J. Lee, S. Lee, K. S. Nahm, P. Kim and S. Jong Yoo, Preparation of porous PtAuCu@Pt core-shell catalyst for application to oxygen reduction, *J. Ind. Eng. Chem.*, 2019, **79**, 210–216.

29 D. Q. Dong, X. Y. Guo, C. L. Ma, L. Y. Gong, L. H. Su, T. Xie, Y. Zhu and J. Wang, Ni-Fe bimetallic core-shell structured catalysts supported on biomass longan aril derived nitrogen doped carbon for efficient oxygen reduction and evolution performance, *Mater. Today Commun.*, 2020, **24**, 101127.

30 N. Cao, J. Su, W. Luo and G. Z. Cheng, Graphene supported Ru@Co core–shell nanoparticles as efficient catalysts for hydrogen generation from hydrolysis of ammonia borane and methylamine borane, *Catal. Commun.*, 2014, **43**, 47–51.

31 S. Liu, Y. T. Li, X. C. Zheng, X. X. Guan, X. L. Zhang and P. Liu, Pd nanoparticles anchoring to core-shell Fe_3O_4@SiO_2-porous carbon catalysts for ammonia borane hydrolysis, *J. Hydrogen Energy*, 2020, **45**, 1671–1680.

32 N. X. Kang, X. R. Wei, R. F. Shen, B. J. Li, E. G. Cal, S. Moya, L. Salmon, C. L. Wang, E. Coy, M. Berlande, J. L. Pozzo and D. Astruc, Fast Au-Ni@ZIF-8-catalyzed ammonia borane hydrolysis boosted by dramatic volcano-type synergy and plasmonic acceleration, *Appl. Catal., B*, 2023, **320**, 121957.

33 L. Yang, J. Su, X. Meng, W. Luo and G. Cheng, *In situ* synthesis of graphene supported Ag@CoNi core-shell nanoparticles as highly efficient catalysts for hydrogen generation from hydrolysis of ammonia borane and methylamine borane, *J. Mater. Chem. A*, 2013, **1**, 10016–10023.

34 M. Rakap, PVP-stabilized Ru–Rh nanoparticles as highly efficient catalysts for hydrogen generation from hydrolysis of ammonia borane, *J. Alloys Compd.*, 2015, **649**, 1025–1030.

35 P. X. Xi, F. J. Chen, G. Q. Xie, C. Ma, H. Y. Liu, C. W. Shao, J. Wang, Z. H. Xu, X. M. Xu and Z. Z. Zeng, Surfactant free RGO/Pd nanocomposites as highly active heterogeneous catalysts for the hydrolytic dehydrogenation of ammonia borane for chemical hydrogen storage, *Nanoscale*, 2012, **4**, 5597–5601.

36 S. Zhang, Y. Shao, H. Liao, M. H. Engelhard, G. Yin and Y. Lin, Polyelectrolyte-induced reduction of exfoliated graphite oxide: a facile route to synthesis of soluble graphene nanosheets, *ACS Nano*, 2011, **5**, 1785–1791.

37 P. Kumar, Harish, G. Andersson, K. M. Subhedar, H. S. Dhami, G. Gupta, A. K. Mukhopadhyay and R. P. Joshi, Utilization of green reductant thuja orientalis for reduction of GO to RGO, *Ceram. Int.*, 2021, **47**, 14862–14878.

38 D. X. Yang, A. Velamakanni, G. Bozoklu, S. Park, M. Stoller, R. D. Piner, S. Stankovich, I. Jung, D. A. Field, C. A. Ventrice Jr and R. S. Ruoff, Chemical analysis of graphene oxide films after heat and chemical treatments by X-ray photoelectron and Micro-Raman spectroscopy, *Carbon*, 2009, **47**, 145–152.

39 H. L. Wang, L. F. Cui, Y. Yang, H. Sanchez Casalongue, J. T. Robinson, Y. Y. Liang, Y. Cui and H. J. Dai, Mn_3O_4 graphene hybrid as a high-capacity anode material for lithium ion batteries, *J. Am. Chem. Soc.*, 2010, **132**, 13978–13980.